Eur Biophys J (2011) 40:835–842
DOI 10.1007/s00249-011-0699-y

ORIGINAL PAPER

Size and conformational features of ErbB2 and ErbB3 receptors: a TEM and DLS comparative study

Ernesto Vicente-Alique · Rafael Núñez-Ramírez · Juan Francisco Vega · Ping Hu · Javier Martínez-Salazar

Received: 17 December 2010 / Revised: 11 March 2011 / Accepted: 17 March 2011 / Published online: 8 April 2011

Abstract ErbB2 and ErbB3 receptors belong to the epidermal growth factor receptor family. The members of this family are able to form homo- and heterodimers that trigger diverse downstream signalling concerned to multiple cellular events. In the absence of a ligand, ErbB3 adopts a characteristic tethered conformation, which differs from ErbB2 extended conformation. In this work, transmission electron microscopy (TEM) and dynamic light scattering (DLS) have been used to characterize the conformational features and the size of ErBb2 and ErbB3 receptors. Two main objectives are presented. The first one is to evaluate the use of TEM as a tool for structural studies for this family of receptors. The low molecular weight of these proteins represents a challenging purpose for TEM studies. The other one is to search for a relationship between the results obtained by TEM and those obtained for the hydrodynamic size measured by DLS. This comparison has allowed us to identify the conformational differences of the receptors and to anticipate the use of these experimental techniques for the study of the ligand activated heterodimerization, a process related to a significant number of human malignancies.

Keywords Epidermal growth factor · ErbB receptors · Transmission electron microscopy · Dynamic light scattering · Conformation · Hydrodynamic size

E. Vicente-Alique · R. Núñez-Ramírez · J. F. Vega (✉) · J. Martínez-Salazar
Departamento de Física Macromolecular, Instituto de Estructura de la Materia, IEM-CSIC C/Serrano 113 bis, 28006 Madrid, Spain
e-mail: jfvega@iem.cfmac.csic.es

P. Hu
Sino Biological Inc., Suite B-310, 14 Zhong He Street, BDA, 100176 Beijing, People's Republic of China

Introduction

The epidermal growth factor receptor (EGFR) family is a model case of receptor tyrosine kinase (RTK). Like other RTK agents, they are activated after ligand binding by the reassembling of the monomers to a homo- and heterodimer receptors that trigger diverse downstream signalling pathways which control multiple cellular events (Fleishman et al. 2002; Moriki et al. 2001; Schlessinger 2000). In the absence of a ligand ErbB1, ErbB3 and ErbB4 adopt a characteristic tethered conformation. On the contrary, the ErbB2 receptor has been shown to be in the extended conformation, being considered as a co-receptor that heterodimerizes with other activated EGFR family members. These structural differences and macromolecular reorganization mechanisms cause a variety of specific monomeric and dimeric macromolecular conformations, which are susceptible of being studied by means of physical methodologies. Some structural features of the EGFR family members have already been studied using different experimental approaches including crystallography and solution small angle X-ray scattering. Crystallography has provided the structural details of both the extracellular region of ErbB1 (Ferguson et al. 2003; Garrett et al. 2003; Ogiso et al. 2002) and its intracellular domain (Stamos et al. 2002; Wood et al. 2004). Structures have also been determined for the extracellular regions of ErbB2 (Cho et al. 2003; Garrett et al. 2003), ErbB3 (Cho and Leahy 2002) and ErbB4 (Bouyain et al. 2005). Small angle X-ray scattering (SAXS) confirmed that the characteristic tethered and extended conformations of the EGFR members are also adopted in solution (Dawson et al. 2007). From all of these studies, a clear difference has been identified between ErbB2 and the rest of the members of the EGFR family, as this receptor has been shown to be in the extended conformation without the action of a ligand. Conversely, ErbB1, ErbB3, and ErbB4 only adopt the

extended conformation after ligand biding activating the dimerization arm. The results obtained lead to higher maximum dimension, D_{max}, of the extracellular region of the ErbB2 receptor obtained from both crystallography and solution SAXS results, than in the rest of the receptors, which is a clear signature of its extended macromolecular conformation.

In our study, we used two different experimental techniques capable of directly evaluating the shape and dimensions of this type of biological system: transmission electron microscopy (TEM) and dynamic light scattering (DLS). TEM has become an essential tool for the study of the structural features of biological macromolecules. The visualization of proteins as isolated particles is easily achievable by means of the negative staining of the samples, a widely used preparation technique as it solves problems related to both the preservation and contrast of the specimens by using solutions of a heavy metal salt. This technique yields results at the nanometer resolution level (Woeste and Demchick 1991; Ohi et al. 2004), making it possible to give accurate results about the shape and size of this type of biological complex, although the drying process during negative staining can produce deformations and changes in conformation in some macromolecular complexes (Llorca 2005). DLS is an absolute, non-invasive and non-destructive technique with applications not only in science but also in industry; a technique mostly applied to the study of the properties of suspensions and solutions of colloids, macromolecules, and polymers. When a monochromatic light beam shines onto a solution of Brownian particles, fluctuations in the scattered light take place. These fluctuations can be used to determine the particle size, in the range from about 1 nm to some microns (Berne and Pecora 2000).

Our objective then is to use both TEM and DLS techniques to study the characteristic macromolecular conformation of the extracellular region of both ErbB2 and ErbB3 receptors linked to Fc region of IgG_1. The Fc domain increases the size of the extracellular domains of ErbB2 and ErbB3 and would lend them a more distinguishable shape. More precisely, the samples have been visualized by TEM in order to obtain the characteristic shape and dimensions of the particles. The measurements obtained on these two complexes have then been compared to DLS data, upon the geometrical considerations obtained by TEM, to explain the values of the experimental hydrodynamic size obtained.

Materials and methods

Samples

Samples used for TEM observation and DLS measurements were recombinant human ErbB2-Fc chimera and ErbB3-Fc chimera (Sino Biological Inc., Beijing, People's Republic of China), supplied as solutions of 0.6–0.7 mg/ml in buffer A (10 mM NaCl, 50 mM Tris and pH 7.5). The recombinant human ErbB2-Fc and ErbB3-Fc comprise 868 and 862 amino acids, respectively, and have calculated molecular masses of 96.1 and 95.4 kDa. For the DLS measurements and in order to eliminate the aggregates, the samples have been further filtered using Nanosep 100 K centrifugal devices (Pall Corporation, Port Washington, NY, USA) with low protein binding membrane to provide reduced non-specific absorption.

Transmission electron microscopy

Different concentrations of protein sample in buffer A were adsorbed directly onto glow-discharged carbon-coated grids. Following negative staining with 2% (w/v) uranyl acetate, the samples were visualized in a JEOL JEM-2100 electron microscope operating at 200 kV (JEOL Ltd., Tokyo, Japan). Grids with optimum particle dispersion and staining were selected for data acquisition. The best concentration for ErbB2-Fc was 0.018 mg/ml and for ErbB3-Fc was 0.0024 mg/ml. Sixty-one and forty-six digital micrographs were recorded, for ErbB2-Fc and ErbB3-Fc correspondingly, under low dose conditions at defocus between 0.8 and 1.5 μm using an Orius Gatan CCD camera (Gatan Inc., Pleasanton, USA) at a final pixel size of 3.3 Å. Different programs from the EMAN package were used for image processing (Ludtke et al. 1999). *Boxer* was used for single-image selection, *proc2d* for image normalization, and the *refine2d.py* algorithm was used for reference-free classification and averaging of the data. In order to interpret the reference-free averages obtained with *refine2d.py*, models of both samples were built from crystallographic structures of ErbB2 and ErbB3 (Cho et al. 2003; Garrett et al. 2003) and Fc domain (Kratzin et al. 1989). Briefly, each extracellular domain structure was computationally fused to the structure of the Fc domain keeping the C-terminus of the extracellular domain of ErbB2 or ErbB3 close to the N-terminus region of Fc domain. These structures were transformed from atomic coordinates to voxels and low-pass filtered to 40 Å of resolution using *Xmipp* (Sorzano et al. 2004) in order to assign the structures of these models to a simple shape (*prolate* or *oblate ellipsoids*) and to facilitate the interpretation of DLS data.

Dynamic light scattering

The DLS measurements were performed in filtered protein solutions using the Zetasizer Nano-ZS (Malvern Instruments, Worcestershire, UK). About 14 μl of the sample was transferred to a clean dust-free microcell. The experiments were done after an equilibration time of 5 min a

temperature of $T = 12 \pm 0.02$°C. The measurements were made avoiding concentration effects. Such effects are due to particle interactions and multiple scattering. To reduce these effects, the measurements were made in the dilute regime and using a non-invasive back scattering technique. In addition, it is also possible to measure the scattered intensity at different depths within the sample in the cell. Measuring in positions close to the cell wall lessens the effect of multiple scattering. In our case, measurement position was varied manually to trace the effect of changing this parameter. No significant difference in experimental data was observed, indicating multiple scattering was not important in our measurements. DLS technique measures the time-dependent fluctuation in the intensity of scattered light that occurs because of the motion of the particles. The analysis of these fluctuations enables the determination of the translational diffusion coefficients, D, of particles, which can be transformed to a size distribution. The value of D is obtained from the fitting of the experimental values of the time correlation function to the following function:

$$g_2(\tau) = A\left[1 + B\exp\left(-2Dq^2\tau\right)\right] \quad (1)$$

where τ is the time, A is the baseline of the correlation function, B is the intercept of the correlation function, $q = [(4\pi n/\lambda)\ \sin(\theta/2)]$ is the scattering vector, n is the refractive index of the solution, λ is the wavelength of the laser, and θ is the scattering angle. A 4-mW He–Ne laser (633-nm wavelength) with a fixed detector angle of $\theta = 173°$ was used. The time-dependence autocorrelation function was acquired every 60 s, with ten acquisitions for each run. From these results, the hydrodynamic diameter, d_H, of the particles is calculated using the Stokes–Einstein equation:

$$d_H = \frac{k_B T}{3\pi\eta D} \quad (2)$$

In this equation, k_B is the Boltzmann's constant, T is the absolute temperature, and η is the solvent viscosity. This equation considers the particles as rigid spheres with a diameter related to the translational diffusion coefficient, which in this instance depends on the size and conformation of the particle at a given temperature and solvent viscosity. The simple exponential model indicated in Eq. (1) yields an overall average, often called the z-average or cumulant average, particle diameter in Eq. (2). In practice, a polynomial fit to the logarithm of the function leads to the size (the first cumulant) and its deviation (the second cumulant), where the polydispersity index PDI corresponds to the square of the normalized standard deviation of an underlying Gaussian size distribution. A more complicated regularization fitting scheme may be used to find the distribution of particle sizes. In our case, the autocorrelation function of the scattered intensity was analyzed by means of inverse Laplace transform by Thikonov analysis (Provencher 1982) using the program SEDFIT (from http://www.AnalyticalUltracentrifugation.com), in order to obtain the size distribution by intensity. In addition, the size distribution by number, obtained from the application of Mie theory, was used for the interpretation of the results (Mie 1908).

Results and discussion

Transmission electron microscopy

Recombinant ErbB2-Fc and ErbB3-Fc were observed under the electron microscope as particles of different shape and size (Fig. 1a, b, respectively, and Table 1). Totals of 4,957 and 5,375 particles of ErbB2-Fc and ErbB3-Fc were manually selected (Fig. 2a). These data sets were classified independently in order to group those images representing similar views of the protein. Each group was rotationally and translationally aligned in order to improve the signal-to-noise ratio of the average image. The reference-free *refine2d.py* algorithm was used to

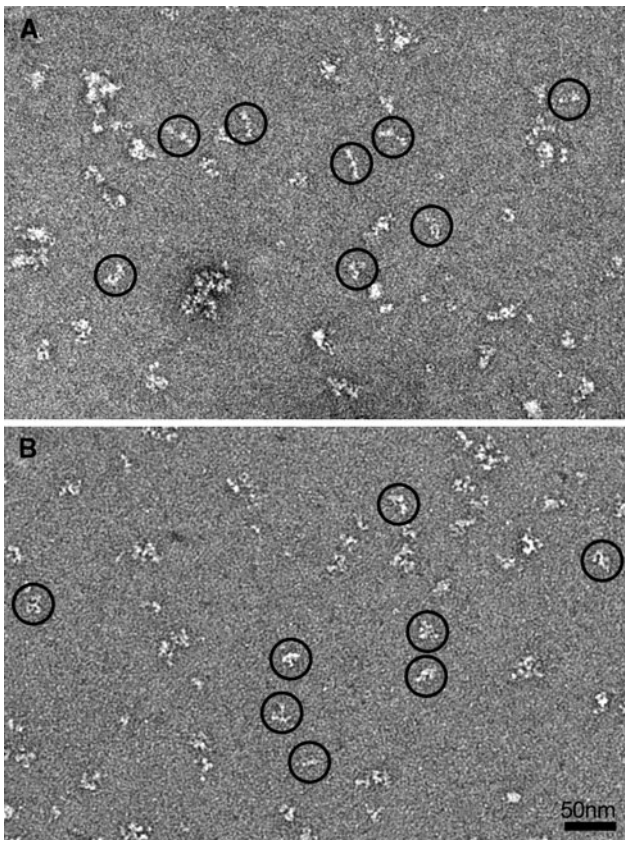

Fig. 1 Representative field from electron micrograph obtained for ErbB2-Fc (**a**) and ErbB3-Fc (**b**). Some representative particles have been *circled*

Table 1 Particle dimensions obtained by TEM of the ErbB2-Fc and ErbB3-Fc proteins studied

	Prolate ErbB2 (nm)	Disk ErbB3 (nm)
TEM	$D_{max} = 15.0$	$D_{max} = 12.0$
	$a = 15.0$	$a \sim 11.0$
	$b = 5.0$	$b = 5.0$

classify and align the images. Representative 2-D averages of each protein are shown in Fig. 2b. ErbB2-Fc average images display an elongated shape with two main masses connected with a small dangling region. ErbB3-Fc average images display a more compact shape with three main masses. In order to evaluate the average images with the known structural data available of these proteins, we built a model for each protein (Fig. 2c). The solved structure of the extracellular domain of ErbB2 and ErbB3 (Cho et al. 2003; Garrett et al. 2003) have been linked to the structure of an Fc domain (Kratzin et al. 1989). The comparison of the average images with different views of ErbB2-Fc and ErbB3-Fc models clearly indicates that the shape and dimension of the reference-free averages are compatible with the known structural data of these samples.

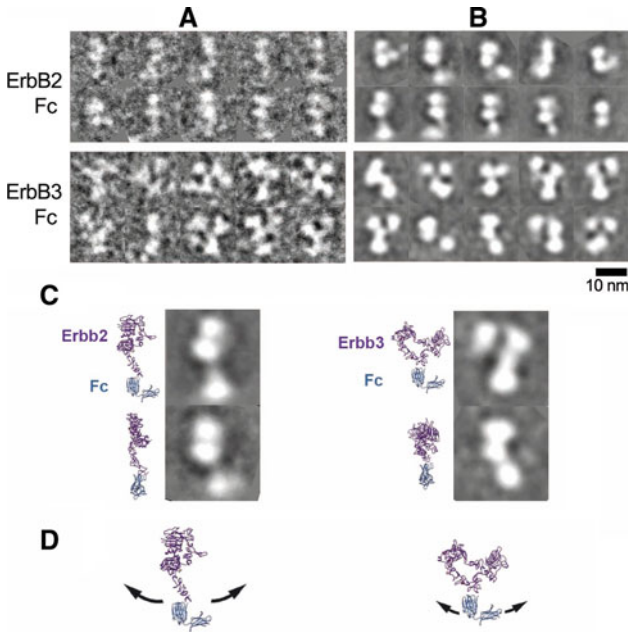

Fig. 2 Classification and alignment of single particles of ErbB2-Fc and ErbB3-Fc. **a** Representative single particles. **b** 2-D reference-free averages. **c** Different views of the structural models for ErbB2-Fc and ErbB3-Fc compared to some reference-free averages shown at the same scale. **d** The reference-free averages of ErbB2-Fc and ErbB3-Fc suggested a high degree of flexibility between both domains, as represented by *arrows*. The structures of the extracellular domain of ErbB2 (Cho et al. 2003; Garrett et al. 2003) and ErbB3 (Cho and Leahy 2002) have been depicted in *magenta* and the structure of the Fc domains (Kratzin et al. 1989) in *blue*

The inspection of the average images of both samples suggests a high degree of flexibility between the extracellular and Fc domains, particularly in the case of ErbB2-Fc case (Fig. 2b, d). This is not surprising since the Fc domain is connected by an unstructured linker, which does not impose a specific domain conformation. This flexibility makes difficult the 3-D combination of the EM images to calculate a map of the structure of each sample. In fact, all attempts of 3-D reconstruction and classification were unsuccessful.

In spite of that, the reference-free averages clearly showed that the macromolecular conformation of these proteins is different. The global dimension of ErbB2-Fc and ErbB3-Fc can be easily visualized using low-pass version (filtered to 40 Å of resolution) of the previously described model (Fig. 3). ErbB2-Fc has the characteristic shape of an elongated ellipsoid with a maximum dimension, D_{max}, of 15 nm. On the contrary, ErbB3-Fc has a conformation closely similar to that of a disk or *oblate ellipsoid*, with $D_{max} = 12.0$ nm. The dimensions of the prolate and oblate particles taken from the images obtained by TEM are given in Table 1. These dimensions are clearly in correspondence with the extended and tethered conformations of ErbB2 and ErbB3 receptor extracellular domains, respectively, as shown by crystallography and SAXS. The value of D_{max} of the macromolecules are 10.5 nm for the tethered ErbB3 and 12.5 nm for the extended ErbB2 structure (Bouyain et al. 2005; Cho and Leahy 2002; Cho et al. 2003; Dawson et al. 2007; Garrett et al. 2003). Obviously, the size increase observed in our

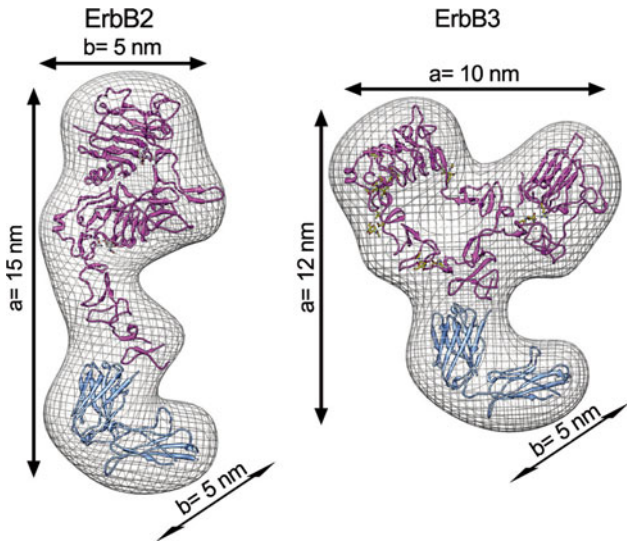

Fig. 3 Three-dimensional model for ErbB2-Fc and ErbB3-Fc. The structure of the models has been low-pass filtered to show a representative envelope of the shape of each macromolecule. The maximum dimensions in width, height, and depth are indicated. The extracellular domains of ErbB2 and ErbB3 have been depicted in *magenta* and the Fc domains in *blue*

ErbB2-Fc and ErbB3-Fc samples obeys the additional Fc segment. Besides, the difference observed between ErbB2-Fc and ErbB3-Fc particles should be readily discernible in the DLS experiments.

Dynamic light scattering

An important parameter characterizing the dynamics of the protein molecules in solution is the translational diffusion coefficient, D, which was determined by DLS from the autocorrelation function as described above (Berne and Pecora 2000). This method also enables us to determine the hydrodynamic dimensions of the proteins and its distribution, providing information about the polydispersity of the sample. The results from the DLS experiments obtained in the samples under study indicate that the intensity correlation function displays two different responses, which cause two intensity distribution peaks in the systems studied. A typical example of these measurements is summarized in Fig. 4 for the ErBb2-Fc sample. To elucidate the importance of the second peak, which corresponds to the larger components, Mie theory (1908) was used to convert the intensity distribution into a number distribution. This treatment of experimental data shows that the second peak nearly disappears upon number distribution analysis. It is well known that DLS experiments are extremely sensitive and even detect traces of large particles, as the scattering intensity of a spherical particle is proportional to the sixth power of its diameter (d^6). In our case, however, the second peak clearly disappears on using the number distribution. Consequently, we believe that the origin of this second peak is due to very small amounts of aggregates or impurities in the sample (Aivaliotis et al. 2003; Mahler et al. 2005; Marchetti et al. 2008; Takata et al. 2000). Anyway, as the TEM methodology treats the particles as numbers, we focus the discussion on the peak observed in the number distribution function. The measurements are highly reproducible, as it can be observed in Fig. 5a. In this case, for the ErBb2-Fc sample an average value of $d_H = 14.0 \pm 0.8$ nm has been obtained, with a standard deviation of <1 nm. Moreover, the polydispersity index is small, with typical values of nearly monodisperse samples. More interestingly, a clear difference is observed when the results of the ErbB2-Fc and ErbB3-Fc samples are compared, as it can be observed in Fig. 5b. As summarized in Table 2, the experimentally determined difference in d_H values by DLS for ErbB2 (14.0 ± 0.8 nm) and ErbB3 (10.5 ± 1.0 nm) also agree with that predicted from crystal structures and from those determined by SAXS in solution. The results support a previous hypothesis that in these conditions, the ErbB2 and ErbB3 proteins adopt the crystallographically defined extended and tethered average conformations, respectively (Dawson et al. 2007). Notwithstanding, it is worth to explore more deeply the relationships between the hydrodynamic size values obtained by DSL and the actual dimensions obtained by TEM. Some procedures have been recently developed concerning the

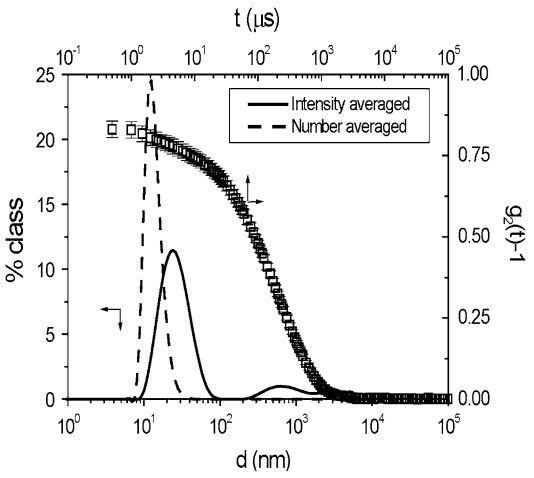

Fig. 4 Intensity time autocorrelation function (*symbols*) and intensity and number size distributions (*lines*) of ErbB2-Fc sample. The result is the average of three independent measurements

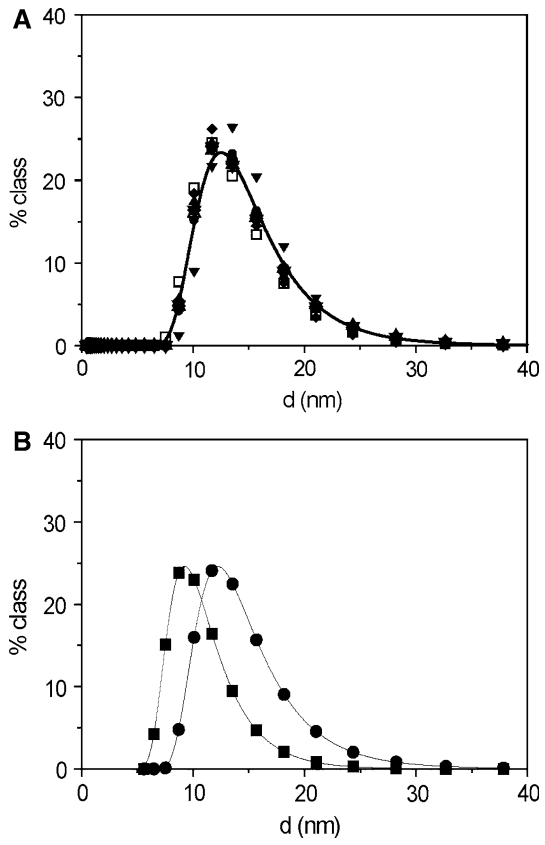

Fig. 5 **a** Percent size distributions of ErbB2-Fc sample obtained from different DLS runs. **b** Comparison of the percent size distributions of (*filled circle*) ErbB2-Fc and (*filled square*) ErbB3-Fc samples

Table 2 Maximum dimension (crystal models and SAXS from the literature) and hydrodynamic diameter d_H of the samples studied

	Crystal structure[a] D_{max} (nm)	SAXS[b] D_{max} (nm)	DLS d_H (nm)	Calculated d_H (nm)
ErbB2	12.5	13.0 ± 0.5	14.0 ± 0.8	*Prolate ellipsoid* 8.0
ErbB3	11.0–11.5	10.5 ± 0.5	10.5 ± 1.0	*Oblate ellipsoid* 9.6

[a] Crystal structure data from Cho and Leahy (2002), Cho et al. (2003), Garrett et al. (2003), Bouyain et al. (2005)

[b] Solution SAXS data from (Dawson et al. 2007)

prediction of the hydrodynamic properties using the information generated from transmission electron microscopy images (García de la Torre et al. 2001). It should be noted that the hydrodynamic diameter obtained in DLS does not only depend on the core size but also on the specific shape of the particles. For a globular/spherical protein, d_H is equal to its diameter, but for non-spherical particles, the measured d_H is equal to the diameter of a sphere that has the same translational diffusion coefficient, inherent to the use of Eq. (2). As judged by the results obtained in TEM images, the particles are not spherical. Therefore, to be able to more directly compare the results obtained by TEM and DLS, we have to adopt different approaches to obtain the value of d_H from the real dimensions of the particles obtained by TEM. From the TEM average images and 3D models, we could visualize ErbB2-Fc particles as *prolated ellipsoids* with the characteristic dimensions (a and b, the major and minor axes, respectively as it is depicted in Fig. 3) given in Table 1. On the other hand, ErbB3-Fc samples have shown a clearly different configuration of protein domains, adopting the shape of *oblate ellipsoids*. The diffusion of ellipsoidal particles was studied in the 1930s by Perrin. For particles with a shape of prolate ellipsoid, the hydrodynamic radius is expressed as (Perrin 1936):

$$d_H = \frac{a(1-x^2)^{1/2}}{\ln\left[\frac{1+(1-x^2)^{1/2}}{x}\right]} \quad \text{with } x = b/a. \tag{3}$$

For particles with a shape of *oblate ellipsoids*, the hydrodynamic diameter reads as:

$$d_H = \frac{b(x^2-1)^{1/2}}{\tan^{-1}\left[(x^2-1)^{1/2}\right]} \quad \text{with } x = a/b. \tag{4}$$

The results of the calculations can be observed in Table 2. A good correlation has been obtained between the calculated and the experimental values in the case of the *oblate ellipsoid* ErbB3-Fc (see Table 2). However, the calculated dimension for the ErbB2-Fc sample is clearly underestimated in comparison to the experimental value obtained from DLS experiments. It is worth to point out here that Eqs. (3) and (4) regard the systems as rigid particles. However, if we focus our attention on Fig. 1b, and d, additional segmental flexibility can be anticipated in the particles, more pronounced in the case of ErbB2-Fc sample. In contrast to rigid particles, systems with segmental flexibility present a variety of conformations, being the equilibrium properties an average over those obtained for each individual conformation (García de la Torre 1994; García de la Torre et al. 2003). In fact, a dichotomy of conformations can be observed in Fig. 1b, mainly in the case of ErbB2-Fc sample. The adopted configurations in solution likely include those in which the Fc segment is closer to the other two masses of the complex, giving rise to an increment of the hydrodynamic size, with respect to that obtained for a *prolate ellipsoid*. Not only the shape plays a role in the value of the hydrodynamic diameter but also the hydrodynamic interactions and the excluded volume effects (García de la Torre 1994). The increase of the size in biological complexes due to additional segmental flexibility has been previously reported by other authors experimentally (Vígh et al. 1989) and by means of computer simulations (Sotriffer et al. 1998), but also a decrease with respect to the rigid particle case has been reported (García de la Torre 1994). In the case of ErbB3-Fc particles, flexibility is also present but it could be limited by the special tethered configuration of the complex.

Then we need to point out that the Fc domain plays a fundamental role as it allows distinguishing between the ErbB2 and ErbB3 extracellular fragments. As it can be observed in Figs. 2 and 3, the Fc fragment gives rise to a clear differentiation between the shapes of both macromolecular species, due also to the fact of the different extended and tethered conformations. If the Fc is eliminated from the structures in Fig. 3, this differentiation between the species is not easy. The changes in the shape and the size of the species under study should be less pronounced in the absence of a substrate like the Fc fragment with a relatively high molecular size. Notwithstanding, these results point to an obvious effectiveness of DLS technique to not only evaluate the hydrodynamic properties of these proteins but also to capture the different behavior of the samples, as a consequence of their different conformational features. In our case, a clear discrimination

between both ErbB2-Fc and ErbB3-Fc complexes is found, in agreement with structural results obtained by means of crystallography (Bouyain et al. 2005; Cho and Leahy 2002; Cho et al. 2003; Garrett et al. 2003) and SAXS (Dawson et al. 2007). Our DLS results are also consistent with those from size exclusion chromatography (data not shown). In view of these results, we can anticipate the application of this technique to study the ligand-binding mechanisms that, in this EGFR family, causes the conformational changes and the homo- and heterodimerization processes. The advantage of this technique is clear, as it can be applied fast and accurately to every protein or biological complex in dilute solution.

Conclusions

The combination of transmission electron microscopy and dynamic light scattering has shown that a clear description of the conformational aspects and size of epidermal growth factor receptors can be done. In agreement with previously reported studies (protein crystal WAXS and protein solution SAXS), without bound ligand, the extracellular region of the receptor ErbB3 adopts a tethered configuration. In this conformation, the particles have a shape close to that corresponding to a disk, with a hydrodynamic diameter of around 10.5 nm. On the contrary, the ErbB2 receptor has shown the clear elongated shape of an ellipsoid. The values of the hydrodynamic diameter measured by DLS are also in agreement with the maximum dimensions obtained in solution SAXS by other authors for these molecules. In addition, in the case of the ErbB3-Fc complex, a close agreement is obtained when the actual dimensions of the particles obtained by TEM are used to calculate the hydrodynamic dimensions from geometrical considerations. The consideration of the rigid particle approach in the ErbB2-Fc case does not work as well as in the ErbB3-Fc complex with the tethered conformation, suggesting a higher segmental flexibility. Then both techniques provide direct valuable conformational and hydrodynamic information, and thus we can anticipate the use of these experimental techniques for the study of the ligand-activated heterodimerization mechanisms, as these processes greatly affect not only by the shape but also the size of the macromolecular complexes.

Acknowledgments This research was funded by the grant MAT2009-12364 from the CICYT (Comisión Interministerial de Ciencia y Tecnología, Spain). JFV acknowledges the CSIC (Consejo Superior de Investigaciones Científicas, Spain) the grant PIE-200850I072. EVA acknowledges the CSIC a JAE-Intro Program fellowship (2010). HP acknowledges the support from members of the Bioprocess Technology team at Sino Biological.

References

Aivaliotis M, Samolis P, Neofotistou E, Remigy E, Rizos AK, Tsiotis G (2003) Molecular size determination of a membrane protein in surfactants by light scattering. Biochim et Biophys Acta 1615:69–76

Berne J, Pecora R (2000) Dynamic light scattering with applications to chemistry, biology and physics. Dover Publications, Mineola

Bouyain S, Longo PA, Li S, Ferguson KM, Leahy DJ (2005) The extracellular region of ErbB4 adopts a tethered conformation in the absence of ligand. Proc Natl Acad Sci 102:15024–15029

Cho HS, Leahy DJ (2002) Structure of the extracellular region of HER3 reveals an interdomain tether. Science 297:1330–1333

Cho HS, Mason K, Ramyar KX, Stanley AM, Gabelli SB, Denney DW Jr, Leahy DJ (2003) Structure of the extracellular region of HER2 alone and in complex with the Herceptin Fab. Nature 421:756–760

Dawson JP, Bu Z, Lemmon MA (2007) Ligand-induced structural transitions in ErbB receptor extracellular domains. Structure 15:942–954

Ferguson KM, Berger MB, Mendrola JM, Cho HS, Leahy DJ, Lemmon MA (2003) EGF activates its receptor by removing interactions that autoinhibit ectodomain dimerization. Mol Cell 11:507–517

Fleishman SJ, Schlessinger J, Ben-Tal N (2002) A putative molecular-activation switch in the transmembrane domain of ErbB2. Proc Natl Acad Sci 99:15937–15940

García de la Torre J (1994) Hydrodynamics of segmentally flexible macromolecules. Eur Biophys J 23:307–322

García de la Torre J, Llorca O, Carrascosa JL, Valpeusta JM (2001) HYDROMIC: prediction of hydrodynamic properties of rigid macromolecular structures obtained from electron microscopy images. Eur Biophys J 30:457–462

García de la Torre J, Pérez Sánchez HE, Ortega A, Hernández JG, Fernandes MX, Díaz FG, López Martínez MC (2003) Calculation of the solution properties of flexible macromolecules: methods and applications. Eur Biophys J 32:477–486

Garrett TPJ, McKern NM, Lou M, Elleman TC, Adams TE, Lovrecz GO, Zhu HJ, Walker F, Frenkel MJ, Garrett TPJ, McKern NM, Lou M, Elleman TC, Adams TE, Lovrecz GO, Kofler M, Jorissen RN, Nice EC, Burgess AW, Ward CW (2003) The crystal structure of a truncated ErbB2 ectodomain reveals an active conformation, poised to interact with other ErbB receptors. Mol Cell 11:495–505

Kratzin HD, Palm W, Stangel M, Schmidt WE, Friedrich J, Hilschmann N (1989) The primary structure of crystallizable monoclonal immunoglobulin IgG1 Kol. II. Amino acid sequence of the L-chain, gamma-type, subgroup I. Biol Chem Hoppe Seyler 370:263–272

Llorca O (2005) Introduction to 3D reconstruction of macromolecules using single particle electron microscopy. Acta Pharmacol Sin 26:1153–1164

Ludtke SJ, Baldwin PR, Chiu W (1999) EMAN: semiautomated software for high-resolution single-particle reconstructions. J Struct Biol 128:82–97

Mahler HC, Müller R, Frieß W, Delille A, Matheus S (2005) Induction and analysis of aggregates in a liquid IgG1-antibody formulation. Eur J Pharm Biopharm 59:407–417

Marchetti S, Sbrana F, Raccis R, Lanzi L, Gambi CMC, Vassalli M, Tiribilli B, Pacini A, Toscano A (2008) Dynamic light scattering and atomic force microscopy imaging on fragments of connecting from human cardiac muscle. Phys Rev E 77:021910

Mie G (1908) Beiträge zur Optik trüber Medien, speziell kolloidaler Metallösungen. Ann Physik 4:377–445

Moriki T, Maruyama H, Maruyama IN (2001) Activation of preformed EGF receptor dimers by ligand-induced rotation of the transmembrane domain. J Mol Biol 311:1011–1026

Ogiso H, Ishitani R, Nureki O, Fukai S, Yamanaka M, Kim JH, Saito K, Sakamoto A, Inoue M, Shirouzu M, Yokoyama S (2002) Crystal structure of the complex of human epidermal growth factor and receptor extracellular domains. Cell 110:775–787

Ohi M, Li Y, Cheng Y, Walz T (2004) Negative staining and images classification: powerful tools in modern electron microscopy. Biol Proc Online 6:23–34

Perrin F (1936) Mouvement Brownien d'un ellipsoide. II. Rotation libre de depolarisation des fluorescence: translation et diffusion de molecules ellipsoidales. J Phys Rad 7:1–11

Provencher SW (1982) A constrained regularization method for inverting data represented by linear algebraic or integral equations. Comp Phys Comm 27:213–227

Schlessinger J (2000) Cell signalling by receptor tyrosine kinases. Cell 103:211–225

Sorzano CO, Marabini R, Velazquez-Muriel J, Bilbao-Castro JR, Scheres SH, Carazo JM, Pascual-Montano A (2004) XMIPP: a new generation of an open-source image processing package for electron microscopy. J Struct Biol 148:194–204

Sotriffer CA, Liedl KR, Linthicum DS, Rode BM, Varga JM (1998) Ligand-induced domain movement in an antibody Fab: molecular dynamics studies confirm the unique domain movement observed experimentally for Fab NC 6.8 upon complexation and reveal its segmental flexibility. J Mol Biol 278: 301–306

Stamos J, Sliwkowski MX, Eigenbrot C (2002) Structure of the epidermal growth factor receptor kinase domain alone and in complex with a 4-anilinoquinazoline inhibitor. J Biol Chem 277:46265–46272

Takata S, Norisuye T, Tanaka N, Shibayama M (2000) Heat-Induced aelation of α-lactoglobulin. 1. Time-resolved dynamic light scattering. Macromolecules 3:5470–5475

Vígh R, Cser L, Kilár F, Simon I (1989) Different segmental flexibility of human serum transferrin and lactoferrin. Arch Biochem Biophys 275:181–184

Woeste S, Demchick P (1991) New version of the negative stain. Appl Environ Microbiol 57:1858–1859

Wood ER, Truesdale AT, McDonald OB, Yuan D, Hassell A, Dickerson SH, Ellis B, Pennisi C, Horne E, Lackey K, Alligood KJ, Rusnak DW, Gilmer TM, Shewchuk L (2004) A unique structure for epidermal growth factor receptor bound to GW572016 (lapatinib): relationships among protein conformation, inhibitor off-rate, and receptor activity in tumor cells. Cancer Res 64:6652–6659